

See discussions, stats, and author profiles for this publication at: <https://www.researchgate.net/publication/339951749>

# Perspective of concentrating solar power

Article in *Energy* · March 2020

DOI: 10.1016/j.energy.2020.117373

CITATION

1

READS

340

7 authors, including:



**Ya-Ling He**

Xi'an Jiaotong University

336 PUBLICATIONS 6,569 CITATIONS

[SEE PROFILE](#)



**Yu Qiu**

Central South University

33 PUBLICATIONS 524 CITATIONS

[SEE PROFILE](#)



**Kun Wang**

Hebei University of Technology

26 PUBLICATIONS 702 CITATIONS

[SEE PROFILE](#)



**Fan Yuan**

Xi'an Jiaotong University

12 PUBLICATIONS 65 CITATIONS

[SEE PROFILE](#)

Some of the authors of this publication are also working on these related projects:



Research on efficient solar concentration, conversion & storage and new power cycles in concentrated solar power [View project](#)



Lattice Boltzmann Predictions for Macroscopic Properties of Porous and Composite Materials [View project](#)

# Perspective of Concentrating Solar Power

Ya-Ling He<sup>\*,a</sup>, Yu Qiu<sup>a,b</sup>, Kun Wang<sup>a</sup>, Fan Yuan<sup>a</sup>, Wen-Qi Wang<sup>a</sup>, Ming-Jia Li<sup>a</sup>, Jia-Qi Guo<sup>a</sup>

\*Corresponding author. E-mail: [yalinghe@mail.xjtu.edu.cn](mailto:yalinghe@mail.xjtu.edu.cn)

*a* Key Laboratory of Thermo-Fluid Science and Engineering of Ministry of Education, School of Energy and Power Engineering, Xi'an Jiaotong University, Xi'an, Shaanxi 710049, China

*b* School of Energy Science and Engineering, Central South University, Changsha, Hunan, 410083, China

**Abstract:** In this perspective paper, the present status and development tendency of concentrating solar power(CSP) are analyzed from two aspects: (1) Potential pathways to efficient CSP through improving operation temperature to above 700 °C; (2) Technologies for efficient solar collection, thermal storage, and power generation at >700 °C. Based on the analyses, barriers on the way to the high-temperature CSP are summarized. They are: (1) the lack of methodology for heliostat design and field layout optimization, (2) significant performance degradations of solar-thermal conversion, heat storage and transfer in receiver and thermal energy storage due to high temperature, (3) the lack of suitable supercritical CO<sub>2</sub>(S-CO<sub>2</sub>) Brayton cycle for CSP and mature design methods for S-CO<sub>2</sub> components. To overcome these issues, perspectives on following three aspects are proposed. Firstly, optimization approaches for optimal heliostat size and layout, and game-changing techniques for heliostat structure design should be brainstormed. Secondly, receivers and thermal storage devices designed through efficiency-improving approaches and fabricated by durable materials should be developed to maintain efficient and reliable operation. Thirdly, the developments of novel S-CO<sub>2</sub> cycle and corresponding key components are eagerly desired to achieve efficient thermal-electric conversion. Perspectives from this paper would present possible approaches to efficient CSP.

**Keywords:** Concentrating solar power; Solar concentrator; Solar receiver; Thermal energy storage; S-CO<sub>2</sub> Brayton cycle

## 1. Introduction

The environmental crisis and energy shortage call for renewable electricity generation [1-3]. In their roadmaps, the European Union (EU), China, and the United States (US) plan to improve their shares of renewable electricity to 100%[4], 80%[5], and 80%[6] in 2050, respectively. Wind and solar energy are two bountiful resources that will play key roles to achieve the goals. In this case, the wind power and solar power will rise to unprecedented high shares.

However, both wind power and photovoltaic power are intermittent, so highly flexible power system is required for keeping the lights on. Any adjustable renewable power that could improve the flexibility of the power system would be valuable. Many previous studies have suggested that

Concentrating Solar Power (CSP) could make it by employing thermal energy storage (TES)[1].

In a CSP plant with TES, solar radiation is concentrated onto a receiver, where the solar energy is converted to thermal energy. A part of the thermal energy is directly utilized to produce high-temperature steam or gas to drive a power cycle for electricity generation. Another part of thermal energy can be stored in a TES unit for driving the cycle at night or under unfavorable weather. Thus, CSP with TES can balance fluctuating power generations, maintaining a reliable power system with high shares of renewables. As a result, the global cumulative CSP capacity has been growing quickly in recent years and has reached 6,430 MW<sub>e</sub> by December, 2019 (see Fig. 1). Moreover, another 3,645 MW<sub>e</sub> is under construction or under development[7-9].

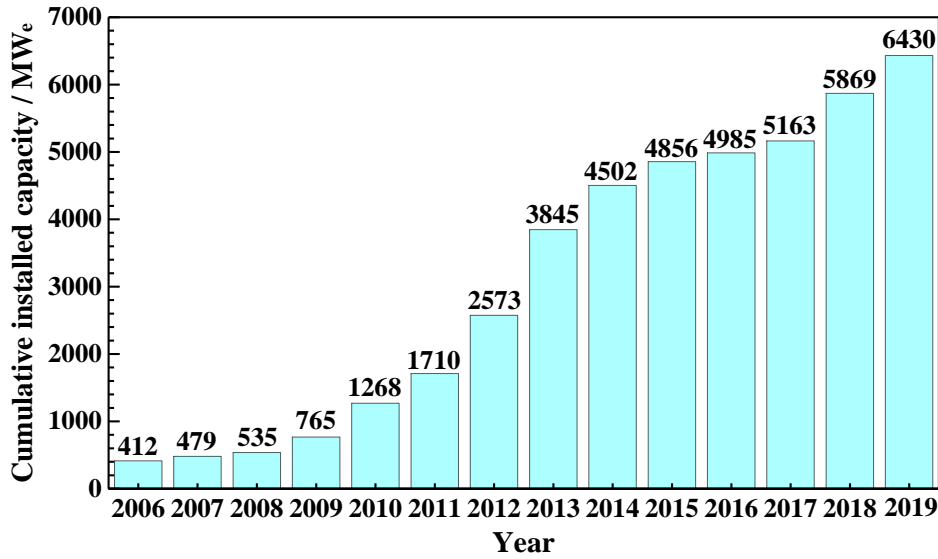


Fig. 1 Global cumulative growth of CSP capacity[7-9].

Despite of its fast development, the installed CSP capacity is still less than 1% of wind and photovoltaic[7]. The major drawback that hinders CSP from large-scale commercialization is the exorbitant nominal levelized costs of electricity (LCOE<sub>nom</sub>, see Eq. S1 in the **Supplementary material**). Although, it is found that some CSP plants can achieve the LCOE<sub>nom</sub> of around 10.9¢·kWh<sub>e</sub><sup>-1</sup> in 2018[10]. The global weighted-average LCOE<sub>nom</sub> ( $\overline{\text{LCOE}}_{\text{nom}}$ , see Eq. S2) of CSP projects commissioned in 2018 is 18.5 ¢·kWh<sub>e</sub><sup>-1</sup>[10], which is much higher than those of photovoltaics (8.5 ¢·kWh<sub>e</sub><sup>-1</sup>) and onshore wind power (5.6 ¢·kWh<sub>e</sub><sup>-1</sup>)[10]. To further reduce the LCOE<sub>nom</sub> of the CSP, the cost reductions and performance improvements for all subsystems in the CSP plant are highly desired.

## 2. Current options and barriers

### 2.1. Concentrating solar power options

The CSP technologies can be divided into parabolic trough collector (PTC)[11], solar power tower (SPT)[12], linear Fresnel reflector (LFR)[13], and power dish collector (PDC)[14] based on

the collector types. According to the types of the thermodynamic cycle and the cycle efficiency, the CSP technologies can be divided into three generations (see Fig. 2). Key information of 168 existing CSP plants and facilities around the world is summarized in the **Supplementary material**.




Generation	1 <sup>st</sup> gen.	2 <sup>nd</sup> gen.	3 <sup>rd</sup> gen.
Receiver outlet temp.	~250 - 450 °C	~500 - 565 °C	~720 °C
Typical plant or technology	PTC, SPT, LFR 	PTC, SPT, LFR 	PDC 
Heat transfer medium	Oil or steam	Steam or salt	Gas
Thermal energy storage	Early designs: No or small Recent designs: Yes	Early designs: No or small Recent designs: Yes	No
Power cycle	Steam Rankine cycle	Stirling	Brayton cycle
Peak temp. of cycle	~240-440 °C	~480-550 °C	~720 °C
Design cycle eff.	~ 28-38%	~ 38-44%	~38%
Annual solar-electric eff.	~ 9-16%	~ 10-20%	~25%

Fig. 2 Different generations of CSP technologies [3, 9, 15-18].

The first-generation CSPs employ Rankine cycle with the design cycle efficiency of ~28-38%, where the peak cycle temperature is as low as 240-440°C, and the PTC, SPT and LFR are usually used. In the early designs, the TES is either not included or negligible, thus the plant can just operate during daytime and sunny condition. In more recent designs, two-tank sensible TES is included to drive the plants at night or cloudy condition, where a binary nitrate salt (60%wt. NaNO<sub>3</sub>-40%wt. KNO<sub>3</sub>) is usually employed as the thermal storage material (TSM). Due to the low cycle efficiency, the annual solar-electric efficiency is just around 9-16% (see Fig. 2). Up to now, the first generation CSPs still represent the majority (80.20%) of the installed capacity, where the trough system contributes to 76.51% (see Fig. 3a).

In most second-generation plants, the PTC, SPT and LFR with the Rankine cycle that has the cycle efficiency of ~38-44% are used, and the peak cycle temperature increases to 480-550°C. Except for a few direct steam generation plants and PDC plants, the TES is included in most newly-built and upcoming second-generation plants, where the binary nitrate is utilized as both the heat transfer material (HTM) and TSM. Due to the higher cycle efficiency, these plants can achieve the annual solar-electric efficiency of around 10-20% (see Fig. 2). Moreover, the PDCs that employ the Stirling cycle with the typical cycle efficiency of ~38% can also be regarded as the second generation. However, only two small PDC plants with the total net capacity of 3 MWe were installed, because the gas leak and other reliability problems of the engine prevent the PDC from commercialization. In

addition, it is clearly illustrated in Fig. 3b that the SPT system is going to be the new trend in the upcoming capacity, which occupies 61.51% of the total capacity.

To further compare the state-of-the-art second-generation CSP technologies, an economic evaluation (See the **Supplementary material**) was conducted under the typical condition in February 2020 using the System Advisor Model (SAM)[19] developed by National Renewable Energy Laboratory. The results in Table 1 show that the second-generation SPT can achieve the lowest  $LCOE_{nom}$  of  $10.90 \text{ ¢} \cdot \text{kWh}_e^{-1}$  among the four CSPs, and it is just 54% higher than the  $7.06 \text{ ¢} \cdot \text{kWh}_e^{-1}$  of the PV. Moreover, SPT also achieves the lowest nominal Levelized Power Purchase Agreement Price ( $LPPAP_{nom}$ ) of  $11.75 \text{ ¢} \cdot \text{kWh}_e^{-1}$  among the four CSPs, and it is 57% higher than the  $7.48 \text{ ¢} \cdot \text{kWh}_e^{-1}$  of the PV. The values of the Internal Rate of Return (IRR) at end of project for four CSPs are within 12.74%-12.75%, which is slightly lower than 12.98% of the PV. These results indicate that the SPT has the potential to generate dispatchable electricity in a more cost-effective way than other CSP systems. Therefore, the SPT is regarded as the leading actor for the third-generation CSP in China, US, and EU, etc. [15-18].

In the third-generation CSP, improving the solar-electric efficiency through increasing the cycle efficiency is regarded as a key approach to reduce the  $LCOE_{nom}$ . The DOE's projects in the US[15], the Next CSP[16] and CSP2[17] projects in the EU, and a national key R&D program of China[18] have recommended the Brayton cycle with the peak cycle temperature of  $>700^\circ\text{C}$  to the next-generation CSP, (see Fig. 2). Meanwhile, the cycle efficiency is expected to be greater than 50%. Three pathways using different HTMs, including molten salt, small particle, and gas, for solar collection have been proposed and regarded as promising candidates by some researchers [15-18]. Up to now, although several small experimental gas plants have been developed, their current efficiencies are still far from the target [20]. Moreover, a 10  $\text{MW}_e$  molten-salt tower plant combined with S- $\text{CO}_2$  Brayton cycle is now under design in China[21].

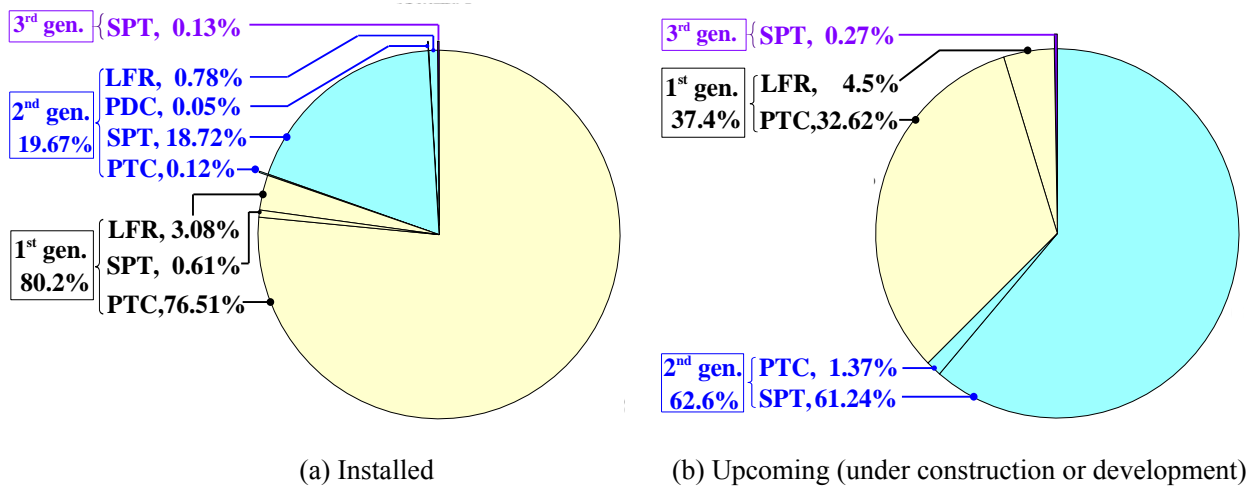


Fig. 3 Installed capacity and upcoming capacity of CSP by Dec. 2019[7, 8].

Table 1 Economic evaluation of four state-of-the-art CSP technologies and PV in Feb. 2020[19]. The designed net capacity of each plant is 100 MW<sub>e</sub>. The location is at Daggett (34.865N, -116.783W).

Item	SPT	PTC	LFR	PDC	PV
Solar multiple	2.4	2.4	2.4	1	1
Heat transfer medium	Solar salt	Solar salt	Solar salt	Gas	-
Receiver outlet temp. / °C	565	525	525	720	-
Energy storage time / h	10 (TES)	10 (TES)	10 (TES)	No	No
Design cycle efficiency / %	41.2	39.7	39.7	~30.5	-
Internal rate of return (IRR) / %	11.0%	11.0%	11.0%	11.0%	11.0%
Year IRR is achieved	20	20	20	20	20
IRR at end of project / %	12.75	12.75	12.75	12.74	12.98
LCOE <sub>nom</sub> (in 2020 USD) / ¢ kWh <sub>e</sub> <sup>-1</sup>	10.90	12.96	15.08	15.12	7.06
LPPAP <sub>nom</sub> (in 2020 USD) / ¢ kWh <sub>e</sub> <sup>-1</sup>	11.75	13.97	16.25	16.07	7.48

## 2.2. Barriers of concentrating solar power

When the temperature is improved to over 700°C in the molten-salt, particle, and gas pathways, challenges occur. Aiming at achieving higher efficiency, better dispatchability, and lower LCOE<sub>nom</sub>, we highlight following barriers that are on the way to the third generation CSP.

(1) There is lack of methodology for heliostat design and field layout optimization to achieve high efficiency, high concentration and low cost when the temperature is higher than 700°C.

(2) Energy transfer and storage performance, and containment materials of the receiver and TES degrade at high temperature, hindering efficiency improvement and cost-effective & safe operation.

(3) Existing cycle layouts of the advanced S-CO<sub>2</sub> Brayton cycle are not completely suitable for the application in CSP, and the key components in the cycle are insufficiently developed.

## 3. Future perspectives

### 3.1. Heliostat field

Heliostat field occupies 40-60% of the capital cost of the tower plant, but it just provides the annual field efficiency of 50-60%[22, 23]. It is clear that the cost reduction and efficiency improvement of the field can make this technology more competitive. To be specific, two approaches, including heliostat design and field layout optimization can help to achieve the above goals.

#### 3.1.1. Heliostat design

A heliostat consists of reflectors, support structures, drivers, and foundation (see Fig. 4). Its performance and cost are influenced by various design factors. To develop efficient and cost-effective heliostats, the following studies (see Fig. 4) are desired to be conducted.

The first task is to find the optimal heliostat size. The larger the heliostat is, the driver cost decreases. However, when the heliostat is too large, the cost of support structures may become significant due to their increasing weight. On the contrary, for small heliostats, the cost of each support structure may be relatively low, but the costs of the foundation, controls and wirings may

become important. Currently operational heliostats cover the size range of 1.1 m<sup>2</sup>-150 m<sup>2</sup> [8]. Although, some studies have obtained their optimal sizes of around 50 m<sup>2</sup>[24, 25] or >200 m<sup>2</sup>[24]. It is clear that no consensus is reached regarding the optimal size, which should be better understood in the future. A similar conclusion has also been drawn by Pfahl et al.[22]

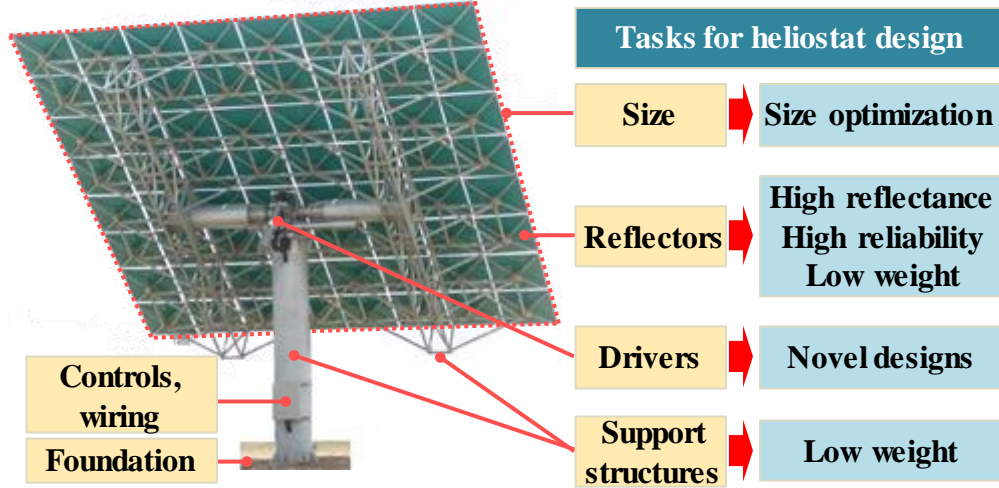


Fig. 4 Components of heliostats and future tasks for heliostat design.

The second task is to refine the reflectors. The 4 mm glass mirror is the current standard reflector, which has the typical slope error and reflectance of 1.3 mrad[26] and 0.935[19], respectively. To further improve the performance, thin-glass and film mirrors are two promising options. A typical sandwich mirror facet, consisting of a 1 mm glass mirror as front layer, a foam core and a 0.5 mm steel back layer, can achieve the slope error of 0.6 mrad and the reflectance of 0.955, which can improve the field efficiency by 4-6% [26]. Although, the sandwich design may increase the cost of the facet. Many studies also show that sandwich facets are strong and very rigid, and can potentially decrease overall cost by reducing the support structure[22, 27]. The film mirror can achieve the reflectance of 0.94 when the slope error is smaller than 1 mrad[28], but it gets scratched easily[29]. In the future, for the both mirrors, the reflectance and reliability should be further improved. Meanwhile, the weight should be reduced.

The third task is to develop low-cost support structures and drivers which contribute 25-35% and 30-35% of the total heliostat cost, respectively[27]. These components are mature technologies, so their manufacturing costs can hardly be reduced, but can be reduced by optimizing the size and reducing the weight. In addition, a fluidic plastic bellows actuator was proposed for the heliostat in Ref.[30], which lightens the weight of support structures and drivers, thus significantly reducing the costs. Although, this actuator has passed the durability testing and was employed in large-scale PV plants. The reliability and life of plastic should be further tested under the realistic condition of tower plant. In the future, more game-changing concepts like this are expected to reduce the costs wherever possible.



### 3.1.2. Heliostat field optimization

The heliostat layout that designs the heliostat positions to maximize the annual field efficiency and minimize the land area is a conundrum with almost indefinite degrees of freedom. However, this problem is usually reduced to several degrees of freedom for simplifying the optimization. Several layouts, including the staggered, biomimetic, heliostat growth, and non-restricted refinement layouts, are commonly employed, as shown in Table 2 [31-36].

Table 2 Summary of typical heliosatat layouts [31-36].

Layouts	Optimizd paramters	Given parameters
Radial staggered layout[31, 32]	Increase in distance of consecutive circles, number of circles between two slip planes, etc.	Heliostat features, security distance between heliostats, the heliostat minimum distance to the tower, heliostat number
Biomimetic layout[34]	$a$ , $b$ in the equations of Fermat's spiral	Same as above
Heliostat growth layout[35]	Location of each heliostat	Heliostat features, tower height, receiver geometry
Non-restricted refinement method[36]	Local posistion refinement of each heliostat	A predefined field

The radial staggered layout (RSL, see Table 2 and Fig. 5a) installs the heliostats around the tower in a staggered way, where a space is introduced after several circles. Tools, like RCELL, DELSOL, Tiesol, MUUEN, and Campo, etc.[32], can be used to design or improve this layout. The biomimetic layout is inspired by the phyllotaxis disc pattern (see Fig. 5). The angular and radial positions of heliostat  $k$  are calculated by  $\theta_k=2\pi\varphi^{-2}\cdot k$  and  $r_k=a\cdot k^b$ , respectively, where  $a$  and  $b$  are necessary to be optimized, and  $\varphi=(\sqrt{5}+1)/2$  [34]. Comparing with the RSL, the annual field efficiency can be improved by 0.36% points with a decrease of 15.8% in the land area[34]. Heliostat growth layout generates the next heliostat at the point with the best the annual available energy after the installation of the previous heliostat. Comparing with a RSL, it can improve the annual field efficiency by 3.9% but the land area increases up to 47%[35]. The non-restricted refinement method can improve a layout generated by other methods. The position of each heliostat is refined one by one by gently adjusting and finding the best position that makes the subfield around the target heliostat achieve the best annual performance. Comparing with a RSL, it can improve the annual collected energy by 0.8%[36].

From current layouts, it is seen that a compromise between the efficiency and land area cannot be easily reached, and we do not even know if there is a possible approach to the optimal design. Therefore, the following studies are suggested: (1) to find new approaches for layout optimization, emphasizing on finding the best degrees of freedom, and (2) to brainstorm novel layout patterns that



exist in the nature.

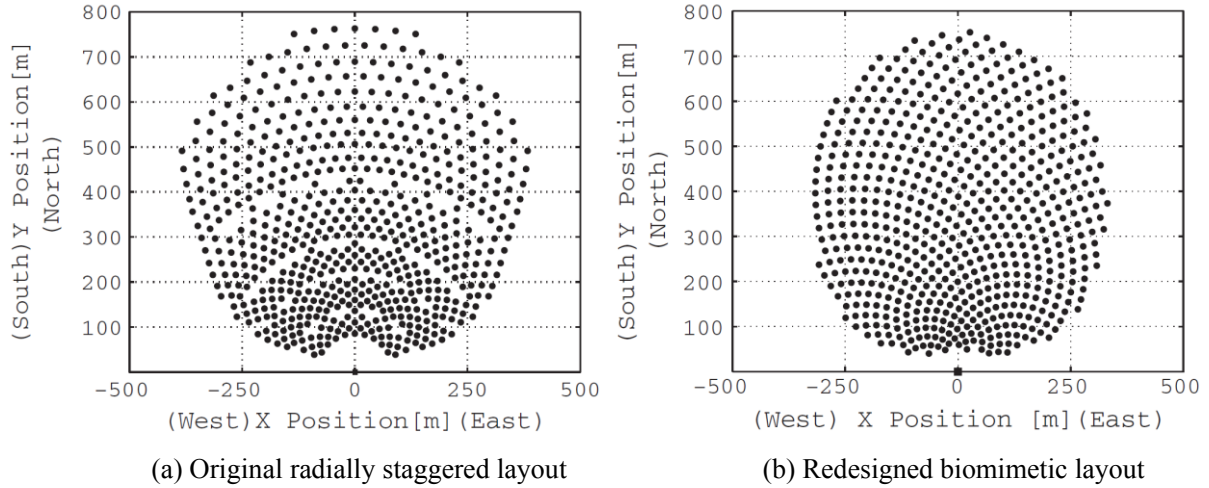


Fig. 5 Comparison of two heliostat layouts for PS10 plant [34].

### 3.2. Solar receiver

Currently, molten salt, particle and gas receivers are considered as three promising receivers in the third-generation CSP plant for temperature greater than 700°C. However, they are still technically immature under such high temperature, facing the issues of material compatibility and efficiency reduction. Therefore, it is essential to solve these problems from the aspects of material selection, receiver design, etc.

#### 3.2.1. Molten salt receiver

The molten salt receiver is the most promising option for the future CSP due to its abundant industrial experience. However, the temperature of higher than 700°C brings significant challenges, including salt decomposition, receiver corrosion and efficiency reduction. To meet these challenges, the following tasks should be further conducted.

The first task is to develop alternative molten salts to replace the binary nitrate (60%wt.  $\text{NaNO}_3$ -40%wt.  $\text{KNO}_3$ ) that would be decomposed above 600°C. Currently, three kinds of salts, which are the carbonates, fluorides and chlorides, are widely suggested as the alternative HTMs, as shown in Fig. 6[37-42]. The fluorides have high thermal conductivity, but they are poisonous and far more corrosive than other two kinds of salts. The carbonates have relatively high density and heat capacity, but they usually contain  $\text{Li}_2\text{CO}_3$  which is quite expensive (7500 USD·ton<sup>-1</sup>)[37]. The chlorides have good thermal performance and low cost. However, the chlorides are highly corrosive at high temperature, especially when water or oxygen exits. Future researches should be focused on modifying the constitution of the salt mixtures to relieve corrosion while maintaining good thermal properties.

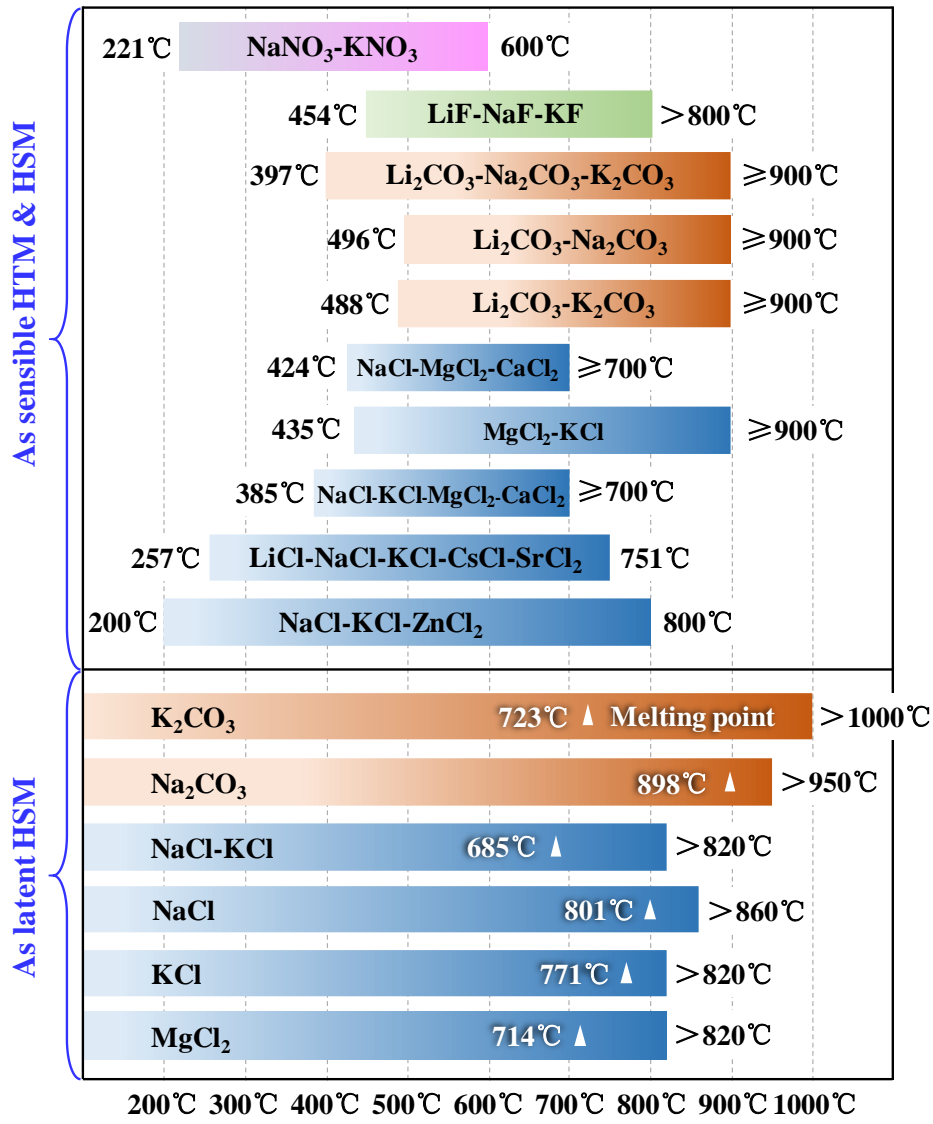


Fig. 6 Operating temperature ranges of molten salts as heat transfer/storage media[37-42].

The second task is to develop corrosion-resisting receiver materials. The typical receiver material Inconel 625 alloy shows a corrosion rate of  $2800 \pm 380 \mu\text{m} \cdot \text{year}^{-1}$  in chloride salt at  $650^\circ\text{C}$ , which is much larger than the commercial requirement of  $<10 \mu\text{m} \cdot \text{year}^{-1}$  [43]. Two potential candidates are the nickel-based alloy and the cermet. For nickel-based alloys, their corrosive characteristics in different salts are still not fully understood. For the cermet, which has been successfully used as the heat exchanger material for chlorides and S-CO<sub>2</sub> at  $800^\circ\text{C}$  in an experiment [1], its corrosion resistance in molten salts is still rarely reported. Moreover, its fabrication and joining methods are still under development. Future researches should be focused on: (1) testing the corrosive characteristics of nickel-based alloys and cermets in the candidate salts; (2) developing novel cermet processing methods, for example, 3D printing. In fact, Sandia National Laboratory (SNL) has successfully fabricated some decimetre-scale prototype receivers by using 3D printing in 2017[44]. Although, current 3D printing still can not fabricate a large salt receiver on the order of ten meters, the industry is now heading in that direction[44].

The third task is to improve the receiver efficiency, which can be decreased by about 6.4% [45] when the outlet temperature increases from 550°C to 700°C for a conventional receiver. A multi-scale design approach (see Fig. 7) can be applied to improve the receiver efficiency by reducing the optical and heat losses[44]. At the macro scale, the conventional receiver ( $\sim 10\text{m}$ ) is replaced by a fin-like receiver (10m-1m) [46], which can reduce the optical loss by trapping the reflected solar rays among the finned structures. The fin-like receiver consists meso-scale tubes with uneven surfaces and turbulators (cm-mm), which can increase the ray absorption at the tube outside and enhance the heat transfer in tube. Moreover, the nano-scale coatings ( $\mu\text{m}$ -nm) with high solar absorptance and low infrared emittance can be deposited on the tubes to further reduce the optical and heat losses[47, 48]. It should be noted that the dust in the air may clog the nano-scale coatings. Some air-blasting equipment may be used to blow the dust away from the receiver surface during the night. Moreover, in the design of the multi-scale receiver, simulation methods can be used. Under the macro- and meso-scale, Monte Carlo ray tracing (MCRT) and computational fluid method (CFD) can be combined to simulate the optical and thermal performance of the receiver[49-51]. In the nano-scale, finite difference time domain (FDTD) method[52] can be adopted to simulate and optimize the optical performance of the coatings.

### 3.2.2. Particle receiver

The particle receiver is another promising option to safely operate above 700°C, where the silica sand, calcined flint clay and ceramic particles, etc. are proposed as the particles to absorb solar radiation[15]. However, different particle materials have different advantages and drawbacks. For example, silica sand and calcined flint clay are stable, abundant and inexpensive, but their solar absorptance are low. The ceramic particles usually have high absorptance, however, they are relatively expensive. Moreover, the abrasion among particles can reduce durability. Therefore, it is necessary to develop abrasion-resisting particles with high absorptance, low emittance and cost.

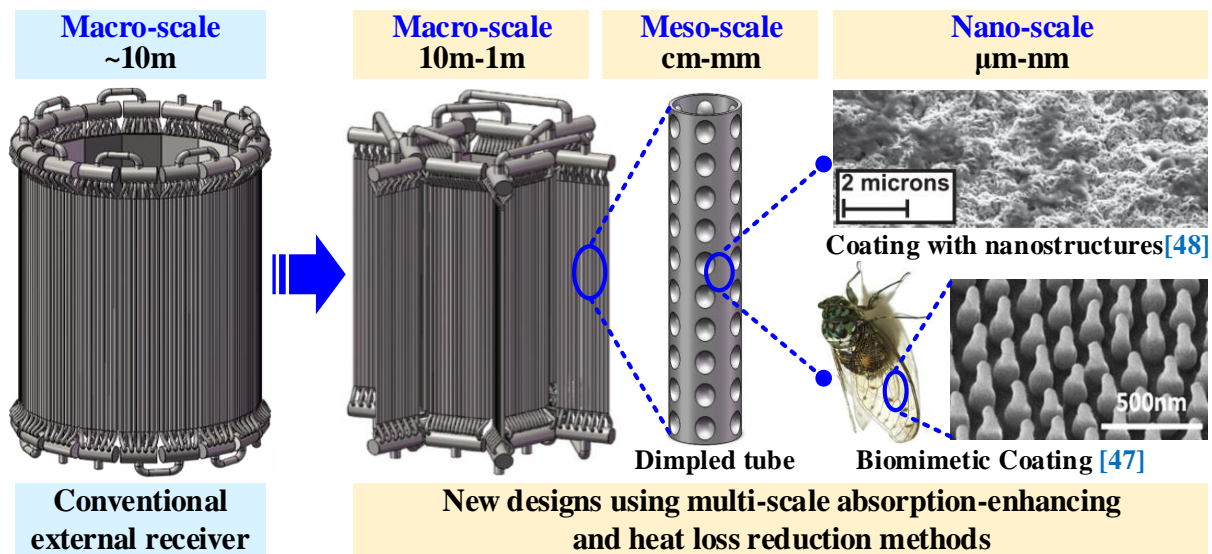


Fig. 7 A multi-scale approach to improve receiver efficiency

The current particle receivers can be categorized to direct and indirect types (see Table 3). Free-falling is a basic form of the direct type, where particles are released from a slot, then heated by the concentrated sunlight. An on-sun test of a 1 MW<sub>th</sub> free-falling receiver shows that the outlet temperature could reach over 700°C, however the receiver efficiency is below 70% [53]. To improve the efficiency, obstructions, such as chevron-shaped mesh structures, can be used to prolong the residence time of the particles within the solar spot and enhance the absorption. Rotating kiln and fluidized bed receivers are other forms of the direct type, which can greatly prolong the residence time to increase the operating temperature above 900°C[54, 55]. However, additional energy is needed to rotate the kiln or fluidize particles. Besides, it is also difficult to maintain a desired mass flow in large scale. Moreover, in the direct type, the particles loss through the aperture can be serious, resulting in increasing heat loss and operating cost. Future researches should be focused on reducing the particle and heat losses by controlling the particle flow, using air curtains or designing novel receiver forms.

Compared with the direct type, indirect type can solve the particle loss problem by flowing the particles in enclosures[56]. However, in the indirect receivers, solar radiation is firstly irradiated on the inner/outer walls of opaque tubes, then carried away in the form of heat by particles that flow along the outer/inner walls. The increased heat transfer resistance from the tube wall to particles can decrease receiver efficiency. Moreover, additional energy is needed to fluidize the particles if a fluidized indirect design is used. In the future, heat transfer between particles and tubes should be further enhanced by optimizing the flow field, designing novel enhanced tubes, etc.

Table 3 Particle receivers[53, 54, 56, 57].

Receiver type	Designs	Outlet temperature	Receiver efficiency
Direct particle receivers	Free-falling	>700 °C	~50%-70%
	Obstructed	>700 °C	~60%-80%
	Rotating kiln	900 °C	75%
	Fluidized bed	>1000 °C	20%-40%
Indirect particle receivers	Gravity-driven flow in enclosures	—	—
	Fluidized flow in opaque tubes	750 °C	—

### 3.2.3. Gas receiver

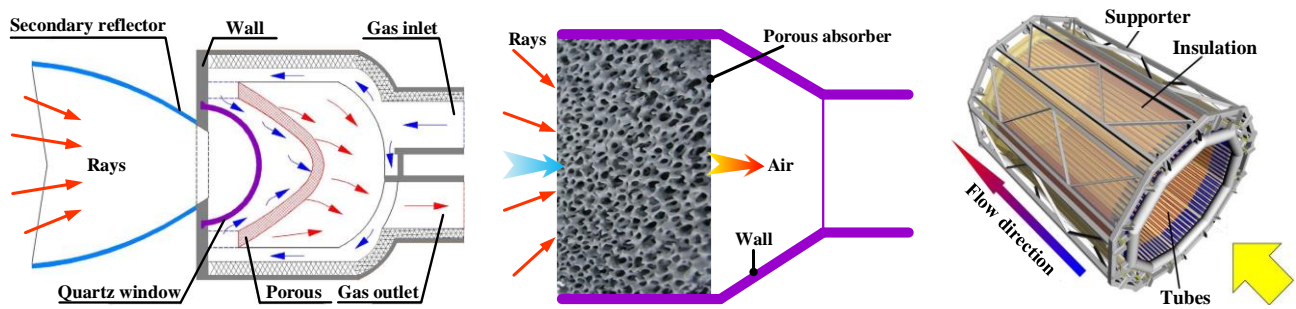
Gas receiver is also a promising receiver technology which can operate at >700°C by using gases as the HTMs, such as air, CO<sub>2</sub>, helium, etc. Similar to the particle receiver, gas receivers can also be categorized into direct and indirect types (see Fig. 8).

Volumetric receivers are typical direct gas receivers, which use porous media to absorb the solar radiation and to heat the gas. The volumetric receivers can be divided into closed-loop and open-loop types (see Fig. 8a,b). In the closed-loop type, the aperture of the receiver is sealed with a quartz

window, and the HTM is not connected to the external air. In the open-loop type, air is directly inhaled from the environment as the HTM. Nowadays, most of the existing closed-loop and open-loop receivers cannot achieve the receiver efficiency of  $>75\%$  at  $>750^{\circ}\text{C}$ , although one experiment stated that the efficiency of  $>80\%$  was achieved at  $1100^{\circ}\text{C}$ [20, 58]. This is mainly due to the poor thermal properties of gases, resulting low heat transfer rate between HTM and porous absorber. To enhance the heat transfer, different porous structures have been developed, including the foam[59], monolithic honeycomb[58], porcupine[60], and gradually-varied porous media[61], etc. Moreover, for the closed-loop type, the stress produced by temperature gradient and the pressure of the HTM may damage the quartz window[59]. Besides, maintaining the seal at an elevated pressure is also a problem, resulting in the operating pressure of  $<2.5\text{ MPa}$ [20, 58] in the exiting closed-loop receivers.

In the third-generation CSP, if the gas with relatively high pressure ( $>2.5\text{ MPa}$ ) is adopted as the HTM, the volumetric receiver will not be applicable. The indirect tubular receiver would be a better choice, where the solar radiation is concentrated on the tube surface to heat the gas flowing in the tube (see Fig. 8c). Many different tubular receivers, such as the cavity[62], fractal-like, flat panel designs[44], etc, were proposed. However, these receivers also suffer from low receiver efficiency. To improve the efficiency, micro-channel receivers have been proposed for increasing the heat transfer area[63]. However, micro channels may cause significant pressure loss. Moreover, most tubular designs are still at the theoretical design stage. Although several experiments have been conducted, the pressure and temperature are far lower than those needed for the future CSP.

After above review, it is suggested that more studies should be focused on (1) increasing receiver efficiency by designing novel receiver structures or optimizing existing candidates, and (2) conducting experiments for the receivers under realistic temperature and pressure conditions to judge their performance.



(a) Direct volumetric receiver: closed-loop (b) Direct volumetric receiver: open-loop (c) Indirect tubular receiver[62]

Fig. 8 Illustrations of typical gas receivers.

### 3.3. Thermal energy storage

The state-of-the-art CSP systems integrate two-tank TES, where the binary nitrate is circulated between hot tank and cold tank, delivering thermal energy at around  $560^{\circ}\text{C}$  to the power block. In the third-generation CSP system with the operating temperature above  $700^{\circ}\text{C}$  for TES, new storage media

will be required. Relevant TES containments and system design should also be revisited to adapt to the high-temperature demand. According to the types of the media, TES falls into two categories, namely the molten-salt TES and the particle TES.

### **3.3.1. Molten-salt TES**

Two main approaches are proposed to develop molten-salt TES for the third-generation CSP. The first one is to use the most mature two-tank design. In this approach, the priority is to explore efficient and low-cost salt composition suitable for the high-temperature environment. The potential salt candidates have been discussed in section 3.2.1. However, all the candidates possess corrosive nature. Moreover, heat loss also indicates severity in the high temperature. Thus excess protection to tank walls and rigorous thermal insulation are required, which will inevitably increase the costs. In this case, the current focus is to explore alternative cost-effective options for both corrosion and heat protection. For example, internal insulation has been proposed to shield the tank wall from inside, which allows the use of low-cost alloys for the tank wall [64].

The two-tank TES can only make use of sensible heat of the salt. As a comparison, latent-heat TES, which is able to absorb/release additional latent heat during phase change, is more advantageous because of the narrow running temperature range ( $150^{\circ}\text{C} \sim 200^{\circ}\text{C}$ ) of S-CO<sub>2</sub> cycle. Some carbonates and chlorides (see Fig. 6) are suitable PCMs possessing appropriate melting temperature and considerable latent heat. However, the main drawback of these PCMs is the low thermal conductivity which is usually below  $2.5 \text{ W} \cdot \text{m}^{-1} \cdot \text{K}^{-1}$  [37]. In fact, heat conduction is the main heat transfer mode for latent-heat TES [65]. Hence the low-thermal-conductivity nature of PCM severely hinders sufficient heat storage/release [66]. To resolve these issues, traditional enhancing methods like adding fins or porous metals have been utilized. Moreover, two aspects of novel methods are also proposed [37]. From material aspect, a small amount of additives such as nanomaterials or expanded graphite have been found to anomalously enhance PCM's thermal property [67]. Further experiments combined with theoretical study into the microscopic enhancement mechanism are still imperative to establish the matching and selection criteria of additives with PCM. From heat reservoir aspect, packed-bed configuration with encapsulated PCM is recommended because of highly-extended heat exchange area [68]. However, reduction measures on encapsulating cost should be adopted before putting into commercialized operation, including the development of alternative low-cost encapsulating materials and methods. Moreover, in the studies of molten-salt TES, simulation methods, such as CFD [69], semi-analytical method [70] and analytical approximation [71], etc., can be used for performance evaluation and optimization.

### **3.3.2. Particle TES**

A typical particle TES is expected to be similar to the two-tank salt TES, except for that particles are used as the heat transfer/storage medium. The expected operating temperature for the hot particle silo is  $800^{\circ}\text{C}$ , and  $350^{\circ}\text{C}$  for the cold silo [72]. The major problems with particle silos are the heat loss

and thermal stress, which can be resolved by the combined design of insulating firebrick and reinforced concrete. However, the lack of practical experience might hide possible technical issues. Moreover, some kinds of particles, like olivine, tend to sinter during long-time storage in the hot silo. Therefore, we suggest two studying topics: (1) further structural optimization for silo design and validation concerning integration with CSP; (2) identification, modification and test on particles to achieve sintering resistance and maintain low cost.

### **3.4. S-CO<sub>2</sub> Brayton cycle**

In recent years, S-CO<sub>2</sub> Brayton cycles have been proposed to replace the conventional water/steam Rankine cycle in CSP. Unfortunately, the suitable cycle layout for CSP application is still not proposed yet, and there even is a lack of a feasible integration approach between the S-CO<sub>2</sub> cycle and other parts of the CSP. Moreover, key components using S-CO<sub>2</sub> as working fluid are also far from mature. Further efforts should be made to address the above issues.

#### **3.4.1 Cycle layout construction and system integration**

There already exists several S-CO<sub>2</sub> Brayton cycle layouts. Fig. 9 illustrates the existing S-CO<sub>2</sub> Brayton cycles and the requirements of the prospective layout for CSP. The original Brayton cycle is very inefficient due to the large amount of waste heat discharged to the surroundings. Therefore, the regeneration is necessary for the Brayton cycle for heat recovery. Recompression cycle layout and precompression are further proposed to avoid temperature pinch-point problem in the recuperator. For further improving the cycle efficiency, intercooling and reheating are also recommended to be incorporated into these cycles [45]. Although, among these layouts, the recompression cycle and the partial cooling cycle are recommended as the most promising cycle layouts for CSP by some studies [73, 74], the existing cycle layouts are far from satisfying the requirements of CSP. They can potentially improve the system efficiency, but their specific work is relatively small. The temperature difference across the solar receiver is also narrow which causes great challenges for coupling with the sensible TES[75]. Therefore, at the current stage, it is an important issue to build an novel S-CO<sub>2</sub> cycle layout that can lead to high efficiency, large specific work and wide temperature difference across the receiver if the mature sensible TES is going to be adopted, or propose an innovative integration approach between S-CO<sub>2</sub> cycles and advanced TES technologies, for example, the latent TES.

Construction of innovative cycle layouts and system integration greatly rely on accurate performance prediction. Most existing models were developed based on steady design-point situation[73-79]. Considering that CSP usually operates under off-design and transient conditions due to fluctuant solar insolation, ambient temperature, and variable load, off-design and dynamic models are highly expected for accurate performance prediction. However, only a few off-design and dynamic models are openly reported[80-82], where constant receiver efficiency or/and constant turbomachinery efficiency are usually assumed. As a result, we suggest that more accurate off-design



and dynamic modeling which greatly depends on the inherently operational curves of turbomachinery, and the receiver dynamic models are needed to be developed.

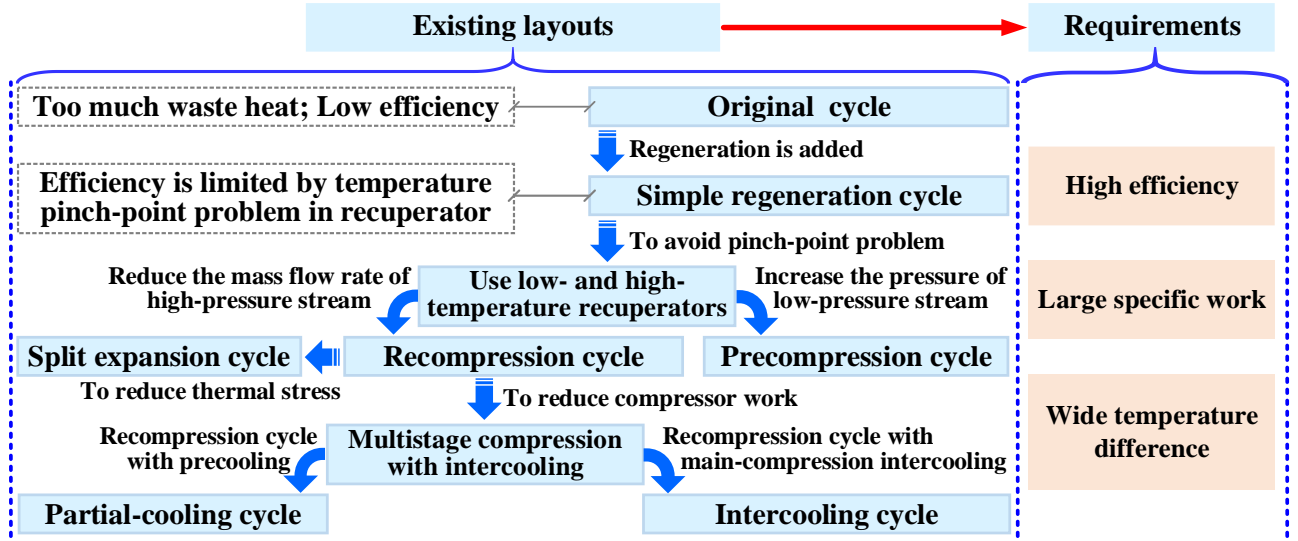


Fig. 9 Existing S-CO<sub>2</sub> Brayton cycles and the requirements of the prospective layouts for CSP.

### 3.4.2 Key S-CO<sub>2</sub> components

Heat exchanger (HX), turbine and compressor are key components in S-CO<sub>2</sub> cycles. Current studies about these components mainly focus on the preliminarily theoretical design and experimental analyses, and there is still a lack of commercial application.

Heat exchange between S-CO<sub>2</sub> and fluids is a necessary process in the S-CO<sub>2</sub> cycle, and the printed circuit heat exchanger (PCHX) that usually employs the straight or zigzag channels is widely suggested for this process due to its high efficiency and compactness. Existing numerical studies on the S-CO<sub>2</sub> HX mainly focus on the channel optimization. Several novel configurations such as S-shape[83] and airfoil[84] channels are proposed for finding a better compromise between the pressure drop and heat transfer. Some experiments were also performed [85, 86], however, there is still a lack of data of HXs operating under the wide ranges of pressure and temperature in S-CO<sub>2</sub> cycle[87]. Moreover, study on dynamic response of S-CO<sub>2</sub> HX is also a hotspot which is the foundation of the dynamic performance prediction and optimization of the system[88, 89]. Some preliminary studies indicate that S-CO<sub>2</sub> PCHX has fast response due to its compactness[90], which is significantly different from traditional HXs. To further improve the PCHX's performance, it is suggested that better channel structures are needed to be explored, and detailed dynamic mechanisms are still necessary to be further investigated.

When particle TES is employed, particle-to-S-CO<sub>2</sub> HX would be the device for releasing heat from the TES. Moving packed-bed heat exchanger (MPB-HX) and fluidized bed heat exchanger (FB-HX) are two widely recommended designs. In the MPB-HXs, including shell-and-tube and shell-and-plate types, dense particle flow driven by gravity flows along tube panels or plates that contain flowing S-CO<sub>2</sub>. The dense particle flow makes particles contact well with the heat transfer surface,

which is helpful to the heat transfer from particles to S-CO<sub>2</sub>. However, the heat transfer is still limited by the relatively low thermal conductivity of the particle bed ( $0.2\text{--}0.6\text{ W}\cdot\text{m}^{-1}\cdot\text{K}^{-1}$ ) [91]. In the FB-HXs, the particles are fluidized using a fluidization gas. Albrecht and Ho [91] pointed out that the heat transfer in the FB-HXs is fundamentally different from that in the MPB-HXs. The fluidized bed can enhance the heat transfer by rapidly refreshing particles cooled by the heat transfer surface with high-temperature particles from the bulk flow, which results in a thin thermal boundary layer[91, 92]. But the disadvantage is that FB-HXs need additional fluidizing power. Currently, several heat transfer models and prototypes have been developed for both types[91, 92], but neither mature MPB-HX nor FB-HX exists for the third-generation CSP. Two research topics are suggested: (1) enhancing heat transfer between flows of particle and S-CO<sub>2</sub> by diminishing stagnation in MPB-HXs or guaranteeing high-efficient fluidization in FB-HXs, (2) developing and evaluating the reliability of heat exchangers under working conditions of the future CSP in a prolonged lifespan.

S-CO<sub>2</sub> compressors and turbines run in ultra-high speed under high pressure in S-CO<sub>2</sub> cycle and will threaten the stability in bearing and sealing, leading to a lower cycle efficiency[93]. Several S-CO<sub>2</sub> test loops have been built to investigate these issues. Cho et al.[94] experimentally tested a S-CO<sub>2</sub> loop using carbon mechanical seals and oil-lubricated bearing, and found that leakage of CO<sub>2</sub> is a significant challenge. Utamura et al.[95] established a 10 kW<sub>e</sub> S-CO<sub>2</sub> loop, and experiments showed that the isentropic efficiency of turbine was 65% at the optimal rotational speed of 100,000 rpm which is much lower than the commonly-used value of 94%[79] in theoretical analysis. Wright et al.[96] performed a 20kW<sub>e</sub> experiment with the turbine and compressor running in 59,000 rpm, which showed the cycle efficiency of only 32.3%. Moreover, it is known that the compressor in the S-CO<sub>2</sub> Brayton cycle consumes much more power than the pump in the steam Rankine cycle[97]. During normal operation, the turbomachinery in the S-CO<sub>2</sub> cycle is self-sustaining, and the turbine can provide sufficient power to drive the compressor. However, during the start-up operation, an external power source is necessary for driving the compressor until the turbine can generate sufficient power[97]. To promote the performance of turbomachinery and S-CO<sub>2</sub> loop, the following studies are suggested: (1) novel bearing and sealing ideas for high pressure and temperature are urgent needed; (2) improving the cycle efficiency through novel design and optimization of the turbine and compressor; (3) developing large-scale experimental loop to verify the feasibility and to gather practical experience of S-CO<sub>2</sub> cycle.

In addition, materials selection is another challenge for the above components when the system operates under extreme condition of 20-30 MPa and 400-700°C, and the combination of material properties, cost, fabricability and availability should be considered. The Ni-base alloys are widely suggested materials[98]. However, the costs would increase dramatically, because the material price would increase from 2-3 \$·kg<sup>-1</sup> of current steel to about 70 \$·kg<sup>-1</sup> of the performance strengthened Ni-base alloys[97]. To find cheaper materials for the S-CO<sub>2</sub> components, some studies have been

focused on ferritic and austenitic steels [99]. In the future, it is necessary to find more candidate materials under S-CO<sub>2</sub> conditions with experimental tests performed.

#### 4. Conclusion

The third-generation CSP tries to improve the solar-electric efficiency and reduce the LCOE<sub>nom</sub> by improving the operation temperature to above 700°C. Currently, some barriers are faced on the way to this high temperature, including the lack of methodology for heliostat design and field layout optimization, significant performance degradation of solar-thermal conversion, heat storage and transfer in receiver and TES due to high temperature, and lack of suitable S-CO<sub>2</sub> cycle layouts and mature design method for S-CO<sub>2</sub> components. Perspectives to remove these barriers are as follows.

(1) Optimization approaches for optimal heliostat size and layout, and game-changing techniques for heliostat design should be brainstormed to obtain efficient heliostat field.

(2) Receiver and thermal storage device designed through efficiency-improving approaches and fabricated by durable materials should be developed to maintain efficient and reliable operation.

(3) Innovative S-CO<sub>2</sub> cycle layouts and their feasible integration approach with CSP should be proposed, and key S-CO<sub>2</sub> components should be developed for the purpose of commercial application.

#### Acknowledge

The study is supported by the Key Project of National Natural Science Foundation of China (No.51436007) and the National Key R&D Program of China(2018YFB1501001).

The authors would also like to thank the Foundation for Innovative Research Groups of the National Natural Science Foundation of China (No.51721004).

#### Appendix: Supplementary data

Supplementary data to this article can be found online at <https://doi.org/10.1016/j.energy.2020.117373>

#### References

- [1] Caccia M, Tabandeh-Khorshid M, Itskos G, Strayer A, Caldwell A, Pidaparti S, et al. Ceramic–metal composites for heat exchangers in concentrated solar power plants. *Nature*. 2018;562:406.
- [2] Liang H, Wang F, Zhang D, Cheng Z, Zhang C, Bo L, et al. Experimental investigation of cost-effective ZnO nanofluid based spectral splitting CPV/T system. *Energy*. 2020;194:116913.
- [3] He YL, Wang K, Qiu Y, Du BC, Liang Q, Du S. Review of the solar flux distribution in concentrated solar power: Non-uniform features, challenges, and solutions. *Appl Therm Eng*. 2019;149:448-74.
- [4] Schellekens G, Battaglini A, Lilliestam J, McDonnell J, Patt A. 100% renewable electricity: A roadmap to 2050 for Europe and North Africa. London: PricewaterhouseCoopers; 2010.
- [5] ERI of NDRC. China 2050 High Renewable Energy Penetration Scenario and Roadmap Study. Beijing: Energy Research Institute (ERI) of National Development and Reform Commission (NDRC); 2015.
- [6] Hand MM, Baldwin S, DeMeo E, Reilly J, Mai T, Arent D, et al. Renewable Electricity Futures Study. Golden, CO: National Renewable Energy Lab.(NREL); 2012, NREL/TP-6A20-52409.
- [7] IRENA. Data & Statistics. International Renewable Energy Agency (IRENA); Accessed time: Jan. 30, 2020, [www.irena.org/Statistics](http://www.irena.org/Statistics).

- [8] NREL. Concentrating solar power projects. National Renewable Energy Laboratory(NREL); Accessed time: Feb. 18, 2020, [www.nrel.gov/csp/solarpaces/index.cfm](http://www.nrel.gov/csp/solarpaces/index.cfm).
- [9] CSP Focus. Project database of global concentrating solar power. CSP Focus; Accessed time: Feb. 18, 2020, [www.cspfocus.cn/en/study/649644246248194048.htm](http://www.cspfocus.cn/en/study/649644246248194048.htm).
- [10] IRENA. Renewable power generation costs in 2018. Abu Dhabi: International Renewable Energy Agency(IRENA); 2019, ISBN 978-92-9260-126-3.
- [11] He YL, Xiao J, Cheng ZD, Tao YB. A MCRT and FVM coupled simulation method for energy conversion process in parabolic trough solar collector. *Renew Energ.* 2011;36:976-85.
- [12] Qiu Y, He YL, Li PW, Du BC. A comprehensive model for analysis of real-time optical performance of a solar power tower with a multi-tube cavity receiver. *Appl Energ.* 2017;185:589-603.
- [13] Qiu Y, Li MJ, Wang K, Liu ZB, Xue XD. Aiming strategy optimization for uniform flux distribution in the receiver of a linear Fresnel solar reflector using a multi-objective genetic algorithm. *Appl Energ.* 2017;205:1394-407.
- [14] Cui FQ, He YL, Cheng ZD, Li YS. Modeling of the dish receiver with the effect of inhomogeneous radiation flux distribution. *Heat Transfer Eng.* 2014;35:780-90.
- [15] Mehos M, Turchi C, Vidal J, Wagner M, Ma Z, Ho C, et al. Concentrating solar power Gen3 demonstration roadmap. Golden, CO: National Renewable Energy Laboratory; 2017, NREL/TP-5500-67464.
- [16] Next-CSP partners. Next-CSP: High Temperature concentrated solar thermal power plant with particle receiver and direct thermal storage. Next-CSP; Accessed time: March 5, 2020, <http://next-csp.eu/about/objectives/>.
- [17] CSP2 partners. Concentrated solar power in particles European project CSP2: Dense suspensions of solid particles as a new heat transfer fluid for CSP. CSP2 project; Accessed time: March 5, 2020, [www.csp2-project.eu/objectives.html](http://www.csp2-project.eu/objectives.html).
- [18] Project partners. Key fundamental issues for the application of S-CO<sub>2</sub> in CSP (National Key R&D Program of China No. 2018YFB1501000). Ministry of Science and Technology of P.R. China; Accessed time: March 5, 2020, [www.most.gov.cn/kjbgz/201907/t20190712\\_147686.htm](http://www.most.gov.cn/kjbgz/201907/t20190712_147686.htm).
- [19] NREL. System Advisor Model Version (SAM ) 2020.1.17. National Renewable Energy Laboratory; Accessed time: 2020, Feb. 17, <http://sam.nrel.gov/download.html>.
- [20] Sedighi M, Padilla RV, Taylor RA, Lake M, Izadgoshasb I, Rose A. High-temperature, point-focus, pressurised gas-phase solar receivers: A comprehensive review. *Energ Convers Manag.* 2019;185:678-717.
- [21] Le Moulec Y, Qi Z, Zhang J, Zhou P, Yang Z, Wang X, et al. Shouhang-EDF 10MWe supercritical CO<sub>2</sub> cycle+ CSP demonstration project. 3rd European conference on supercritical CO<sub>2</sub> power systems 2019, Paris, France, Sept. 19-20, 2019.
- [22] Pfahl A, Coventry J, Röger M, Wolfertstetter F, Vásquez-Arango JF, Gross F, et al. Progress in heliostat development. *Sol Energ.* 2017;152:3-37.
- [23] Lipps F, Vant-Hull L. A cellwise method for the optimization of large central receiver systems. *Sol Energ.* 1978;20:505-16.
- [24] Kolb GJ, Jones SA, Donnelly MW, Gorman D, Thomas R, Davenport R, et al. Heliostat cost reduction study. Albuquerque, NM: Sandia National Laboratories; 2007, SAND2007-3293.
- [25] Pidaparathi A, Hoffmann J. Effect of heliostat size on the levelized cost of electricity for power towers. SolarPACES 2016, Abu Dhabi, Oct. 11-14, 2016.
- [26] Pfahl A, Randt M, Holze C, Unterschütz S. Autonomous light-weight heliostat with rim drives. *Sol Energ.* 2013;92:230-40.
- [27] Coventry J, Campbell J, Xue YP, Hall C, Kim JS, Pye J, et al. Heliostat cost down scoping study-Final Report. Australian Solar Thermal Research Institute; 2016, STG-3261 Rev 01.
- [28] Ganapathi G, Palisoc A, Buchroithner A, Nataraj S, Nesmith B, Kindler A, et al. Development and prototype testing of low-cost lightweight thin film solar concentrator. Asme 10th International Conference on Energy Sustainability,

Charlotte, June 26-30, 2016.

- [29] Ho CK, Sment J, Yuan J, Sims CA. Evaluation of a reflective polymer film for heliostats. *Sol Energ.* 2013;95:229-36.
- [30] Griffith S, Madrone L, Lynn PS, Simon K, McBride J. Fluidic solar actuator. Office USPaT; 2017, US9624911B1.
- [31] Kistler BL. A user's manual for DELSOL3: a computer code for calculating the optical performance and optimal system design for solar thermal central receiver plants. Livermore, USA: Sandia National Labs.; 1986, SAND86-8018.
- [32] Cruz N, Redondo J, Berenguel M, Álvarez J, Ortigosa P. Review of software for optical analyzing and optimizing heliostat fields. *Renew Sust Energ Rev.* 2017;72:1001-18.
- [33] Barberena JG, Larrayoz AM, Sánchez M, Bernardos A. State-of-the-art of heliostat field layout algorithms and their comparison. *Energy Procedia.* 2016;93:31-8.
- [34] Noone CJ, Torrilhon M, Mitsos A. Heliostat field optimization: A new computationally efficient model and biomimetic layout. *Sol Energ.* 2012;86:792-803.
- [35] Sánchez M, Romero M. Methodology for generation of heliostat field layout in central receiver systems based on yearly normalized energy surfaces. *Sol Energ.* 2006;80:861-74.
- [36] Buck R. Heliostat field layout improvement by nonrestricted refinement. *J Sol Energ.* 2014;136.
- [37] Mohan G, Venkataraman MB, Coventry J. Sensible energy storage options for concentrating solar power plants operating above 600 °C. *Renew Sust Energ Rev.* 2019;107:319-37.
- [38] Janz GJ, Allen CB, Bansal NP, Murphy RM, Tomkins RPT. Physical properties data compilations relevant to energy storage. II. Molten salts: data on single and multi-component salt systems. National Standard Reference Data System; 1979, NSRDS-NBS-61-PT-2.
- [39] Qiu Y, Li MJ, Wang WQ, Du BC, Wang K. An experimental study on the heat transfer performance of a prototype molten-salt rod baffle heat exchanger for concentrated solar power. *Energy.* 2018;156:63-72.
- [40] Zhang H, Kong W, Tan T, Baeyens J. High-efficiency concentrated solar power plants need appropriate materials for high-temperature heat capture, conveying and storage. *Energy.* 2017;139:52-64.
- [41] Qiu Y, Li MJ, Li MJ, Zhang HH, Ning B. Numerical and experimental study on heat transfer and flow features of representative molten salts for energy applications in turbulent tube flow. *Int J Heat Mass Tran.* 2019;135:732-45.
- [42] Li P, Molina E, Wang K, Xu X, Dehghani G, Kohli A, et al. Thermal and transport properties of NaCl–KCl–ZnCl<sub>2</sub> eutectic salts for new generation high-temperature heat-transfer fluids. *J Sol Energ.* 2016;138.
- [43] Gomez-Vidal JC, Tirawat R. Corrosion of alloys in a chloride molten salt (NaCl–LiCl) for solar thermal technologies. *Sol Energ Mater Sol C.* 2016;157:234-44.
- [44] Ho CK, Ortega JD, Christian JM, Yellowhair JE, Ray D, Kelton J, et al. Fractal-like materials design with optimized radiative properties for high-efficiency solar energy conversion. Albuquerque, NM: Sandia National Laboratories; 2016, SAND2016-9526.
- [45] Wang K, He YL, Zhu HH. Integration between supercritical CO<sub>2</sub> Brayton cycles and molten salt solar power towers: A review and a comprehensive comparison of different cycle layouts. *Appl Energ.* 2017;195:819-36.
- [46] Wang WQ, Qiu Y, Li MJ, Cao F, Liu ZB. Optical efficiency improvement of solar power tower by employing and optimizing novel fin-like receivers. *Energ Convers Manag.* 2019;184:219-34.
- [47] Huang YF, Jen YJ, Chen LC, Chen KH, Chattopadhyay S. Design for approaching cicada-wing reflectance in low- and high-index biomimetic nanostructures. *ACS nano.* 2015;9:301-11.
- [48] Shah AA, Ungaro C, Gupta MC. High temperature spectral selective coatings for solar thermal systems by laser sintering. *Sol Energ Mater Sol C.* 2015;134:209-14.
- [49] Qiu Y, He YL, Cheng ZD, Wang K. Study on optical and thermal performance of a linear Fresnel solar reflector using molten salt as HTF with MCRT and FVM methods. *Appl Energ.* 2015;146:162-73.
- [50] Qiu Y, He YL, Wu M, Zheng ZJ. A comprehensive model for optical and thermal characterization of a linear Fresnel

- solar reflector with a trapezoidal cavity receiver. *Renew Energ*. 2016;97:129-44.
- [51] Qiu Y, Li MJ, He YL, Tao WQ. Thermal performance analysis of a parabolic trough solar collector using supercritical CO<sub>2</sub> as heat transfer fluid under non-uniform solar flux. *Appl Therm Eng*. 2017;115:1255-65.
- [52] Zhou YP, He YL, Qiu Y, Ren Q, Xie T. Multi-scale investigation on the absorbed irradiance distribution of the nanostructured front surface of the concentrated PV-TE device by a MC-FDTD coupled method. *Appl Energ*. 2017;207:18-26.
- [53] Ho CK, Christian JM, Yellowhair J, Siegel N, Jeter S, Golob M, et al. On-sun testing of an advanced falling particle receiver system. *AIP Conference Proceedings*, AIP Publishing; 2016;1734(1):030022.
- [54] Ho CK. A review of high-temperature particle receivers for concentrating solar power. *Appl Therm Eng*. 2016;109:958-69.
- [55] Wu W, Trebing D, Amsbeck L, Buck R, Pitz-Paal R. Prototype testing of a centrifugal particle receiver for high-temperature concentrating solar applications. *J Sol Energ*. 2015;137:041011.
- [56] Martinek J, Ma Z. Granular flow and heat-transfer study in a near-blackbody enclosed particle receiver. *J Sol Energ*. 2015;137:051008.
- [57] Benoit H, López IP, Gauthier D, Sans J-L, Flamant G. On-sun demonstration of a 750°C heat transfer fluid for concentrating solar systems: Dense particle suspension in tube. *Sol Energ*. 2015;118:622-33.
- [58] Ávila-Marín AL. Volumetric receivers in Solar Thermal Power Plants with Central Receiver System technology: A review. *Sol Energ*. 2011;85:891-910.
- [59] Du BC, Qiu Y, He YL, Xue XD. Study on heat transfer and stress characteristics of the pressurized volumetric receiver in solar power tower system. *Appl Therm Eng*. 2018;133:341-50.
- [60] Karni J, Kribus A, Rubin R, Doron P. The “porcupine”: a novel high-flux absorber for volumetric solar receivers. *J Sol Energ*. 1998;120:85-95.
- [61] Du S, Ren Q, He YL. Optical and radiative properties analysis and optimization study of the gradually-varied volumetric solar receiver. *Appl Energ*. 2017;207:27-35.
- [62] Korzynietz R, Brioso JA, del Río A, Quero M, Gallas M, Uhlig R, et al. Solugas – Comprehensive analysis of the solar hybrid Brayton plant. *Sol Energ*. 2016;135:578-89.
- [63] Ho CK. Advances in central receivers for concentrating solar applications. *Sol Energ*. 2017;152:38-56.
- [64] Jonemann M. Advanced thermal storage system with novel molten salt: December 8, 2011-April 30, 2013. Golden, CO: National Renewable Energy Laboratory; 2013, NREL/SR-5200-58595.
- [65] Tao YB, Liu YK, He YL. Effect of carbon nanomaterial on latent heat storage performance of carbonate salts in horizontal concentric tube. *Energy*. 2019;185:994-1004.
- [66] Tao YB, He YL. A review of phase change material and performance enhancement method for latent heat storage system. *Renew Sust Energ Rev*. 2018;93:245-59.
- [67] Yuan F, Li MJ, Qiu Y, Ma Z, Li MJ. Specific heat capacity improvement of molten salt for solar energy applications using charged single-walled carbon nanotubes. *Appl Energ*. 2019;250:1481-90.
- [68] Li MJ, Jin B, Ma Z, Yuan F. Experimental and numerical study on the performance of a new high-temperature packed-bed thermal energy storage system with macroencapsulation of molten salt phase change material. *Appl Energ*. 2018;221:1-15.
- [69] Li MJ, Qiu Y, Li MJ. Cyclic thermal performance analysis of a traditional Single-Layered and of a novel Multi-Layered Packed-Bed molten salt Thermocline Tank. *Renew Energ*. 2018;118:565-78.
- [70] Ma Z, Li MJ, Yang WW, He YL. General performance evaluation charts and effectiveness correlations for the design of thermocline heat storage system. *Chem Eng Sci*. 2018;185:105-15.
- [71] Bechiri M, Mansouri K. Analytical solution of heat transfer in a shell-and-tube latent thermal energy storage system. *Renew Energ*. 2015;74:825-38.
- [72] Calderón A, Palacios A, Barreneche C, Segarra M, Prieto C, Rodriguez-Sanchez A, et al. High temperature systems

using solid particles as TES and HTF material: A review. *Appl Energ.* 2018;213:100-11.

- [73] Neises T, Turchi C. A Comparison of Supercritical Carbon Dioxide Power Cycle Configurations with an Emphasis on CSP Applications. *Energy Procedia.* 2014;49:1187-96.
- [74] Turchi CS, Ma Z, Neises TW, Wagner MJ. Thermodynamic study of advanced supercritical carbon dioxide power cycles for concentrating solar power systems. *J Sol Energ.* 2013;135:041007.1-41007.7.
- [75] Wang K, He YL, Zhu HH. Integration between supercritical CO<sub>2</sub> Brayton cycles and molten salt solar power towers: A review and a comprehensive comparison of different cycle layouts. *Applied Energy.* 2017;195:819-36.
- [76] Wang K, Li MJ, Guo JQ, Li PW, Liu ZB. A systematic comparison of different S-CO<sub>2</sub> Brayton cycle layouts based on multi-objective optimization for applications in solar power tower plants. *Applied Energy.* 2018;212:109-21.
- [77] Padilla RV, Soo Too YC, Benito R, Stein W. Exergetic analysis of supercritical CO<sub>2</sub> Brayton cycles integrated with solar central receivers. *Applied Energy.* 2015;148:348-65.
- [78] Binotti M, Astolfi M, Campanari S, Manzolini G, Silva P. Preliminary assessment of sCO<sub>2</sub> cycles for power generation in CSP solar tower plants. *Applied Energy.* 2017;204:1007-17.
- [79] Wang K, He YL. Thermodynamic analysis and optimization of a molten salt solar power tower integrated with a recompression supercritical CO<sub>2</sub> Brayton cycle based on integrated modeling. *Energy Convers Manag.* 2017;135:336-50.
- [80] Osorio JD, Hovsapien R, Ordonez JC. Dynamic analysis of concentrated solar supercritical CO<sub>2</sub>-based power generation closed-loop cycle. *Applied Thermal Engineering.* 2016;93:920-34.
- [81] Coquard R, Rochais D, Baillis D. Experimental investigations of the coupled conductive and radiative heat transfer in metallic/ceramic foams. *Int J Heat Mass Tran.* 2009;52:4907-18.
- [82] Dyreby JJ, Klein SA, Nellis GF, Reindl DT. Modeling Off-Design and Part-Load Performance of Supercritical Carbon Dioxide Power Cycles. 2013.
- [83] Wen ZX, Lv YG, Li Q, Zhou P. Numerical study on heat transfer behavior of wavy channel supercritical CO<sub>2</sub> printed circuit heat exchangers with different amplitude and wavelength parameters. *Int J Heat Mass Tran.* 2020;147:118922.
- [84] Wang WQ, Qiu Y, He YL, Shi HY. Experimental study on the heat transfer performance of a molten-salt printed circuit heat exchanger with airfoil fins for concentrating solar power. *Int J Heat Mass Tran.* 2019;135:837-46.
- [85] Bae SJ, Kwon J, Kim SG, Son I-w, Lee JI. Condensation heat transfer and multi-phase pressure drop of CO<sub>2</sub> near the critical point in a printed circuit heat exchanger. *International Journal of Heat and Mass Transfer.* 2019;129:1206-21.
- [86] Pidaparti SR, Anderson MH, Ranjan D. Experimental investigation of thermal-hydraulic performance of discontinuous fin printed circuit heat exchangers for supercritical CO<sub>2</sub> power cycles. *Exp Therm Fluid Sci.* 2019;106:119-29.
- [87] Xu J, Liu C, Sun E, Xie J, Li M, Yang Y, et al. Perspective of S-CO<sub>2</sub> power cycles. *Energy.* 2019;186:115831.
- [88] Kwon JS, Bae SJ, Heo JY, Lee JI. Development of accelerated PCHE off-design performance model for optimizing power system operation strategies in S-CO<sub>2</sub> Brayton cycle. *Applied Thermal Engineering.* 2019;159:113845.
- [89] Padilla RV, Too YCS, Benito R, Stein W. Exergetic analysis of supercritical CO<sub>2</sub> Brayton cycles integrated with solar central receivers. *Appl Energ.* 2015;148:348-65.
- [90] Jiang Y, Liese E, Zitney SE, Bhattacharyya D. Design and dynamic modeling of printed circuit heat exchangers for supercritical carbon dioxide Brayton power cycles. *Appl Energ.* 2018;231:1019-32.
- [91] Albrecht KJ, Ho CK. Design and operating considerations for a shell-and-plate, moving packed-bed, particle-to-sCO<sub>2</sub> heat exchanger. *Sol Energ.* 2019;178:331-40.
- [92] Farsi A, Dincer I. Thermodynamic assessment of a hybrid particle-based concentrated solar power plant using fluidized bed heat exchanger. *Sol Energ.* 2019;179:236-48.
- [93] Li MJ, Zhu HH, Guo JQ, Wang K, Tao WQ. The development technology and applications of supercritical CO<sub>2</sub> power cycle in nuclear energy, solar energy and other energy industries. *Appl Therm Eng.* 2017;126:255-75.



- [94] Cho J, Shin H, Ra HS, Lee G, Roh C, Lee B, et al. Research on the development of a small-scale supercritical carbon dioxide power cycle experimental test loop. The 5th International Symposium-Supercritical CO<sub>2</sub> Power Cycles, San Antonio, March 28-31, 2016.
- [95] Utamura M, Hasuike H, Yamamoto T. Demonstration test plant of closed cycle gas turbine with supercritical CO<sub>2</sub> as working fluid. *Strojarstvo: časopis za teoriju i praksu u strojarstvu*. 2010;52:459-65.
- [96] Wright SA, Radel RF, Vernon ME, Rochau GE, Pickard PS. Operation and analysis of a supercritical CO<sub>2</sub> Brayton cycle. Albuquerque: Sandia National Laboratories; 2010, SAND2010-0171.
- [97] Brun K, Friedman P, Dennis R. Fundamentals and applications of supercritical carbon dioxide (sCO<sub>2</sub>) based power cycles. Cambridge: Woodhead publishing; 2017.
- [98] Walker M, Stapp D, Hinze J. Collective summary of sCO<sub>2</sub> materials development part II: high-temperature alloy corrosion behavior within compact heat exchangers. Livermore: Sandia National Laboratory; 2019, SAND2019-14554R.
- [99] Pint BA, Thomson JK. Effect of oxy-firing on corrosion rates at 600-650° C. *Materials and Corrosion*. 2014;65:132-40.